Available online at www.sciencedirect.com
SCIENCE DIRECT
Journal of Catalysis 230 (2005) 186–194
JOURNAL OF CATALYSIS
www.elsevier.com/locate/jcat

High-pressure X-ray photoelectron spectroscopy of palladium model hydrogenation catalysts. Part 1: Effect of gas ambient and temperature

D. Teschner [a,b,*], A. Pestryakov [a], E. Kleimenov [a], M. Hävecker [a], H. Bluhm [a], H. Sauer [a], A. Knop-Gericke [a], R. Schlögl [a]

[a] *Fritz-Haber-Institut der MPG, Faradayweg 4-6, D-14195 Berlin, Germany*
[b] *Institute of Isotope & Surface Chemistry, CRC, Hungarian Academy of Sciences, P.O. Box 77, Budapest, H-1525 Hungary*

Received 2 September 2004; revised 26 November 2004; accepted 29 November 2004

Abstract

In light of accumulating evidence highlighting the major effect of operational conditions (gas composition, pressure, temperature) on the surface/bulk structure of catalytic materials, their characterization should involve more and more in situ methods. We constructed a synchrotron-based high-pressure X-ray photoelectron spectroscopic (XPS) instrument, allowing us to investigate the surface and near-surface state of a catalyst in the mbar pressure range. We discuss here the surface characteristics of palladium samples as a function of gas phase (hydrogen, oxygen) and temperature. We demonstrate that the surface region of catalytic materials behaves dynamically in its composition, always reflecting its environment. For example, surface oxide can be formed on Pd(111) in oxygen, which decomposes rapidly when the gas supply is switched off. The chemical nature of carbonaceous deposits also depends strongly on the operational conditions (gas-phase hydrogen, temperature). This is the first time that an XPS investigation of palladium β-hydride was performed at RT. The possible drawbacks of using a non-UHV setup (e.g., fast carbon accumulation) are also discussed.

Keywords: High-pressure XPS; Palladium; Hydrogen; Carbonaceous deposits; Surface oxide; Palladium hydride

1. Introduction

Palladium is one of the most important hydrogenation catalysts; it is widely employed in industrial processes [1–7] and in basic research [8–23]. Its practical importance in the reaction of various gases has stimulated wide-spread investigations from the point of view of catalytic [8–12,14,15,17] and surface properties [13,16,18–23].

The field of hydrogen-metal interaction, including chemisorption, relaxation, reconstruction, and hydrogen dissolution, is an extremely well-studied area of surface science [20–33]. The energetics of hydrogen adsorption and dissolution in palladium (involvement of highly coordinated sites on the surface and in subsurface positions) is well established, but only for "clean, surface science" conditions. For "dirty," real catalytic environments, hardly any direct (spectroscopic) information is available, even though there are an enormous number of papers reporting on the major role of the partial pressure of hydrogen in various catalytic processes [12,34–37]. The role of hydrogen in these processes is still one of the important challenges to mechanistic studies. The major drawback in investigating hydrogen-containing systems is the very low sensitivity of the spectroscopic methods toward hydrogen.

Carbonaceous deposits on metal surfaces represent a natural state of precious metal catalysts. Numerous species of carbon are observed on the surface of catalysts, ranging from carbides to hydrogen-rich aliphatic polymers. The chemical

* Corresponding author. Fax: +49 30 8413 4676.
E-mail address: teschner@fhi-berlin.mpg.de (D. Teschner).

0021-9517/$ – see front matter
doi:10.1016/j.jcat.2004.11.036

states of accumulated carbonaceous species on model palladium surfaces have often been a matter of debate [38–42]. The majority of these studies were performed ex situ or in ultrahigh vacuum (UHV), far from real catalytic conditions (this is often referred to as an example of the "pressure gap").

In the last decade, the development of in situ characterization methods [43–49] helped researchers to gain a better understanding of a working catalyst. In situ studies provided evidence that the surface structure and the valence state of an active component can be very different in situ compared with UHV conditions, and weakly bonded adsorbed species or subsurface/bulk-solved components can be present under relevant catalytic conditions. The interaction of adsorbates with subsurface and bulk species can be essential for effective catalytic turnovers, and the specific interplay between surface and subsurface/bulk species is mainly controlled by the operational conditions. Therefore in situ techniques should play a crucial role in catalytic investigations. X-ray photoelectron spectroscopy (XPS) is one of the most widely used techniques; it is very powerful because of its surface sensitivity. Conventionally, XPS is operated at UHV pressures, since the emitted photoelectrons are strongly scattered in a gas phase. However, identification of the weakly adsorbed species and surface carbon present *during the catalytic run* is difficult in UHV-XPS, as the mere evacuation induces desorption or can change the chemical state of the surface species via loss of hydrogen [50–52]. To overcome these limitations, high-pressure XPS chambers were designed in the late 1970s [50]. A number of high-pressure XPS experiments have been performed since then [53–57]. Our in situ XPS setup employs differentially pumped electrostatic lenses that allow us to measure the sample in a gaseous environment (flow-through mode) at pressures of up to 5 mbar.

We report here data collected with a Pd(111) single crystal and polycrystalline palladium foil. Part I of this paper is meant to be an introductory article pinpointing the possibilities and drawbacks of using high-pressure XPS with palladium and concentrating on the effects of experimental conditions (hydrogen pressure, oxygen, temperature) on the surface state of palladium samples. In the second part, as a further step, we present a real "in situ" study to get a better understanding of the hydrogenation processes, with *trans*-2-pentene as a model reactant.

2. Experimental

The in situ XPS experiments were performed at beam lines U49/2-PGM1 and UE56/2-PGM2 at BESSY in Berlin. Our setup operates analogously to the instrument described in Ref. [58]. A differentially pumped electrostatic lens system is the key feature of our setup, allowing us to investigate the sample in the mbar pressure region. The sample position is controlled by a 3D manipulator, and the sample is placed $\sim$ 20 mm from the X-ray window and $\sim$ 2 mm in front of the first aperture, which is the entrance to the electrostatic lens system. The surface normal of the sample is parallel to the optical axis of our lens system, and incidence X-rays irradiate the sample at an angle less than 55° from the surface normal. C 1s and Pd 3d spectra were recorded with photon energies of $h\nu = 660$ and 720 eV (electron kinetic energy $\sim$ 370 eV), respectively (if not otherwise stated). Valence band spectra were obtained with a photon excitation of 150 eV. The overall spectral resolution measured by argon (Ar 2p) was about 0.2 eV at both beamlines. The binding energies were calibrated against the Fermi level of the samples. Decomposition of the C 1s region was performed with the use of Gauss convoluted Doniach–Sunjic curves (DS*) [59]. The Pd 3d peaks were fitted with the use of Gauss–Lorentz profiles with exponential tail. The latter gave a much better agreement with the experimental data (better chi-square values) than the often used DS* function. The atomic composition was calculated with the use of energy-dependent photoionization cross sections [60], assuming a homogeneous distribution of the various elements in the information depth. The inelastic mean free path for the electron energy used is approx. 9 Å for palladium and 13 Å for carbon [61]. No impurity other than carbon was observed; thus %(C 1s) + %(Pd 3d) = 100%. Pd(111) single crystal and polycrystalline palladium foil (Goodfellow, purity 99.99%) were investigated in this study. We mounted the samples on a temperature-controlled heater and cleaned the hydrocarbon contamination from them by first heating them in oxygen (10^{-4} mbar, 973 K) and then flushing to 1073 K in vacuum. Because of the residual gas pressure of 10^{-7} mbar in our chamber, the sample was always covered by some hydrocarbon contamination. Gas flow into the reaction cell was controlled with calibrated mass flow controllers and leak valves. The pressure in the experimental cell was varied from high vacuum (10^{-7} mbar) up to 4 mbar, and the sample was investigated at temperatures from 298 to 623 K. The experimental cell was connected to a transfer chamber where treatments could be carried out in the 10^{-6} mbar to 1 bar pressure range. The following procedure was used for the preparation of palladium β-hydride. First, we cleaned the carbon contamination from a piece of Pd foil by sputtering and oxygen treatment (473 K, 0.15 mbar), and then the surface oxide was decomposed by evacuation. Hydrogen (1 bar) was introduced, and the sample was kept at 338 K for 20 min and then cooled down RT. After 1 h of atmospheric hydrogen treatment, the pressure was slowly decreased to 2.3 mbar, and under this controlled ambient the sample was transferred back to the experimental chamber, where we set the hydrogen pressure at the same level as used previously.

3. Results

Before we go into a detailed analysis of the spectra, we would like to consider a phenomenon that is not present in conventional XPS measurements. When Pd was measured

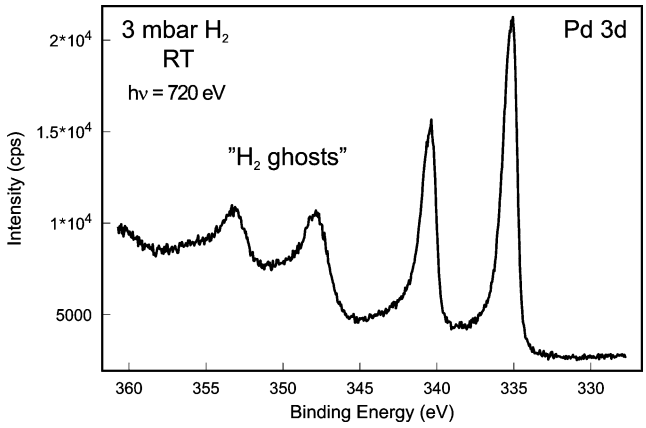

Fig. 1. Pd 3d region of palladium foil in the presence of 3 mbar hydrogen.

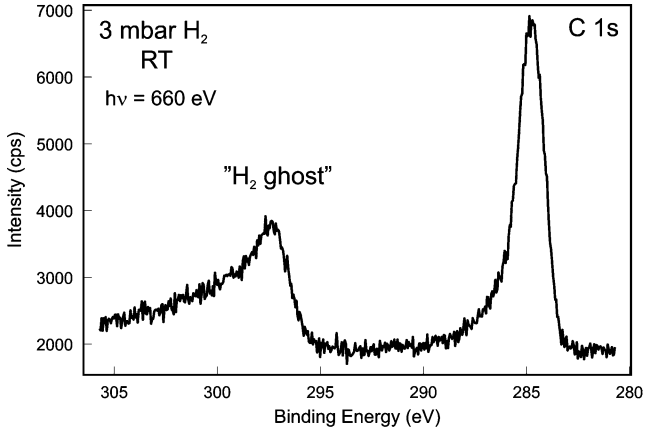

Fig. 2. C 1s region of palladium foil in the presence of 3 mbar hydrogen.

in hydrogen, additional peaks appeared in the spectra; the relative intensity of the new peaks showed a positive correlation with the introduced hydrogen pressure. Figs. 1 and 2 show the Pd 3d and the C 1s regions in the presence of 3 mbar hydrogen at room temperature. In addition to the expected peaks, additional peaks at higher BE (i.e., lower KE) are present in the spectra. The energy separation of the original and the additional peaks is constant (∼ 12.7–12.8 eV), and the new peaks are strongly broadened at the high-energy side. The correlation of the peak intensity with the H_2 pressure and the energy separation indicates that the new peaks are due to the inelastic scattering of the photoelectrons on the hydrogen molecules. During this process the hydrogen 1s electrons are excited mainly to the 2p state ($E = 12.6$ eV) but also to higher Rydberg transitions, as well as to the vacuum continuum ($E > 15.4$ eV).

When palladium foil is measured without treatment in vacuum, the carbon content within the probing depth in our experiments is larger than 95%. After a cleaning cycle (see Section 2) the C content decreased to 30%, which is still a high value. Part of this residual carbon was most probably present during the cleaning procedure (not removed) in grain boundaries, but part of it might originate from the readsorption from the residual contaminants in the chamber

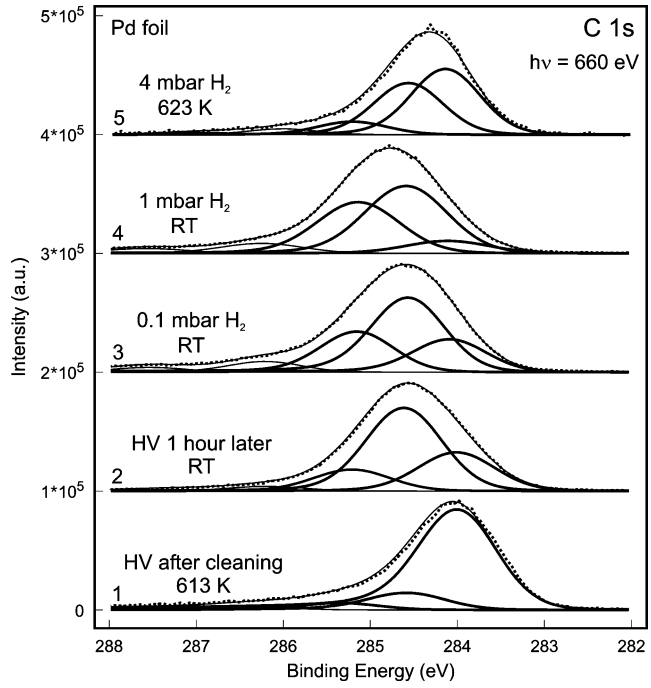

Fig. 3. C 1s region of palladium foil at different experimental conditions. Incident photon energy, $h\nu = 660$ eV. Dashed line: measured data, full line: fits.

atmosphere during the cooling period. The base pressure in our experimental cell is $\sim 10^{-7}$ mbar (although mainly water), which makes it difficult to prepare and maintain clean (carbon-free) metal surfaces in nonoxidizing environments. Consequently, we observe carbon accumulation over time at our base pressure of 10^{-7} mbar (Fig. 3, curves 1 and 2), without the intentional direct introduction of any hydrocarbons. However, in a separate experiment under oxidizing conditions (0.06 mbar O_2 at 300 °C), we were able to prepare a clean Pd surface on a Pd(111) single crystal (Fig. 5). In oxygen (0.06 mbar O_2, 573 K), the Pd 3d peak contains a contribution from bulk Pd (BE = 335.0 eV) and two additional components at BEs of 335.6 and 336.3 eV (energy separation of +0.6 and +1.3 eV), whereas the C 1s region does not show the presence of any carbon (not shown). The Pd 3d peak with a BE of 335.6 eV might be due to adsorbed oxygen, and the 336.3-eV peak could be due to PdO [62,63]. However, recently [64] a new surface oxide phase Pd_5O_4 was identified on Pd(111) with exactly the same BE spacing as observed here, and thus we identify the high BE peaks as being due to Pd_5O_4. The surface oxide phase in Ref. [64] was prepared at 573 K by exposing the Pd(111) surface to 3000 L of oxygen (5×10^{-6} mbar for 600 s), but after that the temperature was quenched to RT, at which point the Pd 3d spectrum was recorded. When the oxygen flow is switched off in our experiment (still at 573 K), the oxide phase is quickly removed (∼ 15% of the oxide might be still there, calculated from the decrease in the 335.6-eV peak area), and the spectrum resembles the well-known pattern with a surface core level shift of about −0.3 eV. Fifteen minutes after

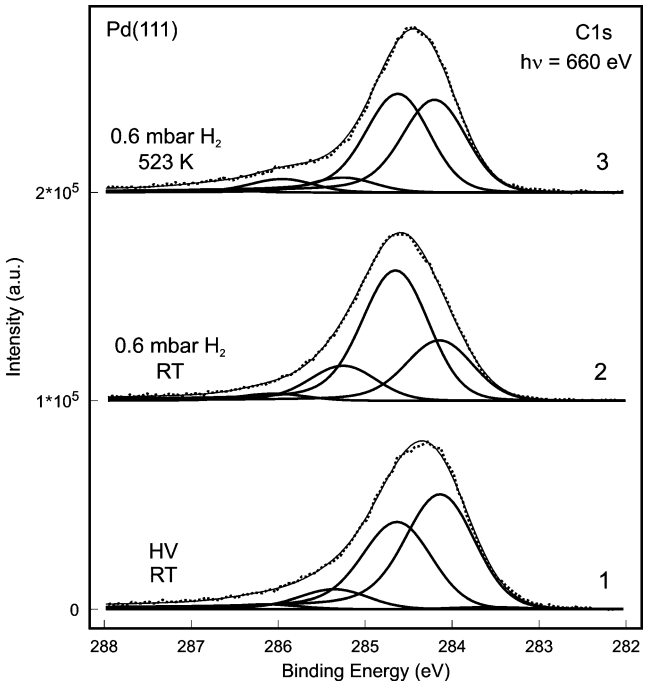

Fig. 4. C 1s region of Pd(111) single crystal at different experimental conditions. Incident photon energy, $h\nu = 660$ eV. Dashed line: measured data, full line: fits.

Table 1
The main carbon types, their signs used in the text and their binding energy positions

C type	Sign	BE (eV)
Carbon connected to palladium	C–Pd	284.1 ± 0.05
Carbon connected to carbon	C–C	284.55 ± 0.05
Carbon connected to hydrogen	C–H	285.2 ± 0.05

the oxygen is switched off, the surface already contains a few percent carbon. When the temperature is decreased the accumulation of C on the surface increases further.

When Pd foil was kept in high vacuum for 1 h and the temperature was decreased from 613 K to room temperature, the amount of carbon doubled, the position of the maximum shifted by +0.5 eV to 284.55 eV, and the peak became broader (Fig. 3). The carbon accumulation was slightly enhanced by the high flux of the synchrotron beam. Introduction of hydrogen shifted the C 1s peak further toward higher BE, and the amount of carbon increased as well. Increasing the temperature (350 °C) in hydrogen ambient shifted the peak back toward lower binding energies. Even higher hydrogen pressure (4 mbar) was not able to compensate for this effect. The carbon content in 4 mbar H_2 at 623 K decreased to 70% (−10%). The total amount of carbon measured on Pd(111) was generally less than that on the foil (30–40% vs. 70–80%). The trends in the C content observed as a function of hydrogen pressure and temperature, however, were similar for foil and single crystal (Fig. 4). The measured spectra were analyzed with a least-squares fitting procedure. For this analysis we used more than one main carbon component for several reasons. Since the absolute binding energy scale can be calibrated quite accurately (±0.01 eV), binding energy shifts of up to 0.75 eV could be observed. Second, although the C 1s peaks were not well resolved, their shapes were markedly different. Third, the full width at half-maximum (FWHM) varied also (up to ∼ 25%). And last but not least, depth-profiling experiments (see Part II) also revealed the presence of different carbon species, as the shape of the C 1s peak changed with the photon energy, thus yielding spectra with different information depth. To be able to satisfactorily fit the main C 1s region (283–286 eV), we needed at least three components for the analysis. The binding energies for these three main components were found to be at 284.1 ± 0.05, 284.55 ± 0.05, and 285.2 ± 0.05 eV. The exact identification of these species is not unambiguous; however, according to the literature [65–68], they correspond to (chain) carbon that is likely attached by several bonds to the metal, to graphitic carbon, and to aliphatic carbon containing hydrogen, respectively. Since the chemical shift of the different species reflects their chemical environment, and since in our system we have three main elements (Pd, C, H), we will use the following nomenclature for these three main carbon components (Table 1): carbon connected to palladium, C–Pd (BE = 284.1 eV); carbon connected to carbon, C–C (BE = 284.55 eV); and carbon connected to hydrogen, C–H (BE = 285.2 eV). The small peaks found above 286 eV correspond to some oxygen-containing carbon.

Initially, after a cleaning procedure and above 573 K, mainly C–Pd is present (Fig. 3, curve 1). This carbon is most probably one- or two-dimensional (atomically dispersed or in islands) and obviously has very low hydrogen content. According to theoretical calculations [69], the binding energy of atomically dispersed carbon at a surface or subsurface location is in the range of 284–284.5 eV. Thus one part of this C–Pd species may represent subsurface carbon. During the carbon accumulation from the background, the initial "layer" starts to assemble, and when the amount of carbon is high enough, three-dimensional structures form (high contribution of graphitic carbon, Fig. 3, curve 2). When the surface is then exposed to hydrogen, mainly the C–Pd-type carbon is transferred to the C–H type (Fig. 3, curves 3 and 4), whereas heating induces loss of hydrogen (Fig. 3, curve 5; Fig. 4, curve 3). Interestingly, the effect of the presence of 4 mbar hydrogen seems to be negligible compared with the effect of heating, since the C–H component at this stage was very low. High temperature favors the formation of C–Pd-type carbon. Carbon on palladium single crystal shows the same general behavior as that observed for the foil; however, its ability to transform C–Pd to C–H is much smaller.

Figures 6 and 7 show the complementary Pd 3d data for the C 1s spectra discussed above. The spectrum of the clean surface from Fig. 5 is also included in Fig. 7 for better comparison. Mainly three types of metallic palladium species are discussed in the literature [19,70], namely clean surface palladium atoms (surface core level shift) with a BE of $3d_{5/2}$ ∼ 334.7 eV, bulk palladium at ∼ 335.0 eV, and

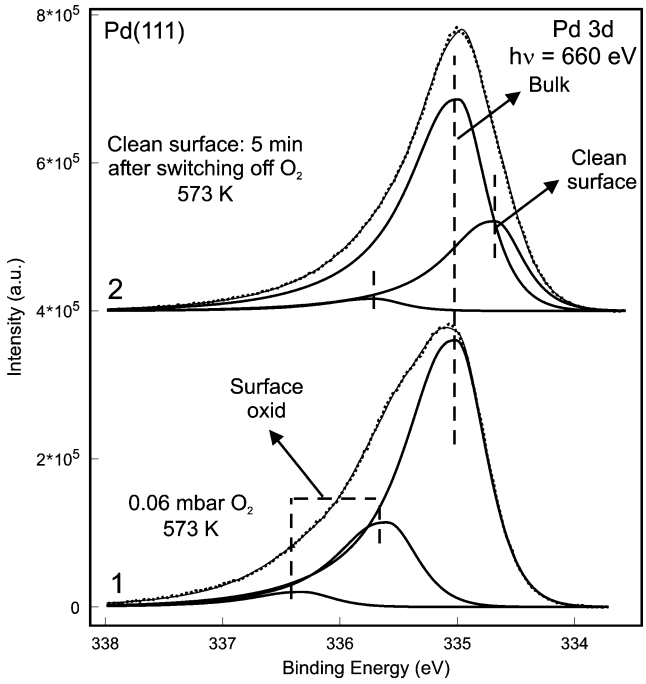

Fig. 5. Pd $3d_{(5/2)}$ region of Pd(111) single crystal in the presence of 0.06 mbar O_2 at 573 K (1) and right after switching off O_2 (2). Incident photon energy, $h\nu = 660$ eV. Dashed line: measured data, full line: fits.

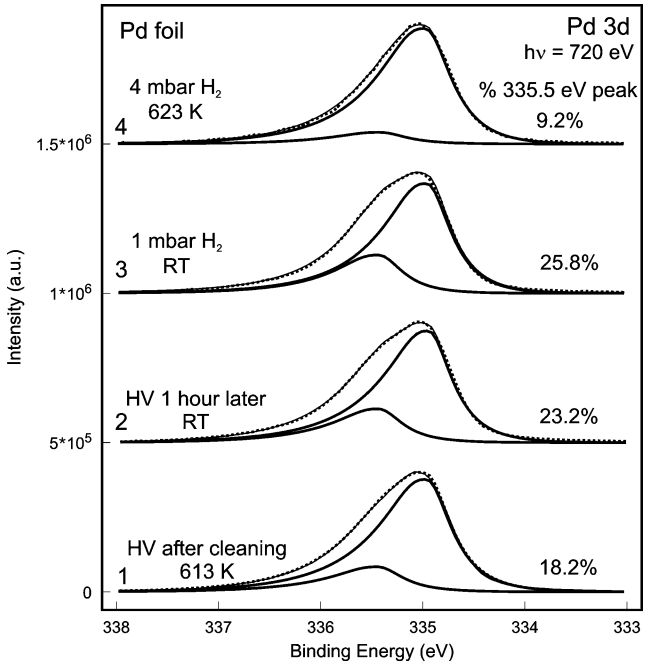

Fig. 6. Pd $3d_{(5/2)}$ region of palladium foil at different experimental conditions. Incident photon energy, $h\nu = 720$ eV. Dashed line: measured data, full line: fits. The relative intensity of the 335.5 eV component is also included.

surface palladium atoms covered by (or bonded to) different types of adsorbed species. Binding energies for the last type were found in the range of 335.3–335.6 eV. Since our palladium is always covered by some type of carbon (under nonoxidizing conditions), it is not surprising that our Pd 3d

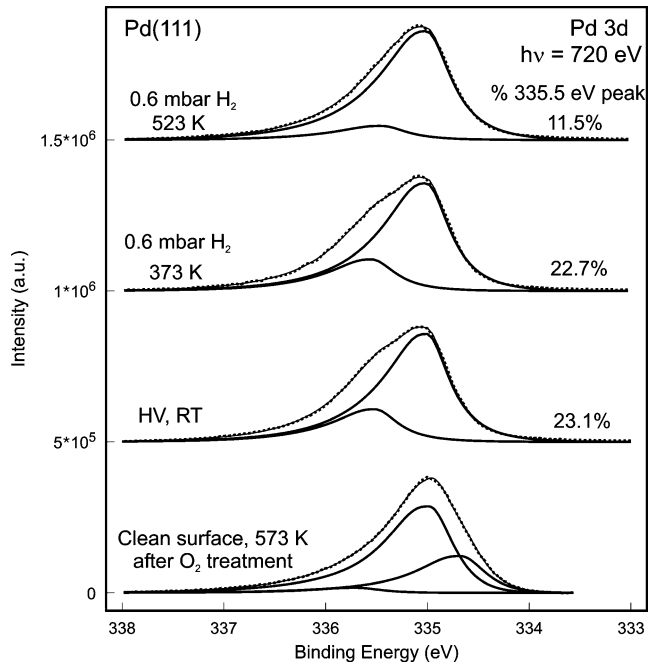

Fig. 7. Pd $3d_{(5/2)}$ region of Pd(111) single crystal at different experimental conditions. Incident photon energy, $h\nu = 720$ eV (except that after O_2 treatment, 660 eV). Dashed line: measured data, full line: fits. The relative intensity of the 335.5 eV component is also included.

least-squares fits did not show a component at ∼ 334.7 eV (SCLS). Thus the Pd 3d core level peaks were fitted only by two components; bulk Pd and adsorbate-induced Pd. After cleaning in high vacuum, the adsorbate-induced surface peak was already present. Its intensity increases during the carbon accumulation period. Its highest intensity was reached in hydrogen ambient (Fig. 6, curve 3), when the total amount of carbon was highest as well. Interestingly, temperature treatment (623 K) removed most of this component; the lowest level (9.2%) of this component was reached under those conditions, even though the total carbon content was still 70%. Here again, Pd(111) behaves in a manner quite similar to that of the Pd foil. It is interesting to mention, however, that although the relative amount of the adsorbate-induced surface Pd peak is rather comparable for the two samples at steady high-vacuum and high temperature (Pd foil: 23.2 and 9.2%; Pd(111): 23.1 and 11.5%), the total amount of carbon is roughly twice as high for the Pd foil. In light of the above data, the total amount of carbon cannot be correlated with the adsorbate-induced surface Pd component.

Since we have seen that it was impossible to correlate the adsorbate-induced surface Pd peak with the total amount of carbon, we have plotted the main carbon components as a function of the relative abundance of the Pd 3d 335.5 eV peak (Fig. 8). It is difficult to draw unambiguous conclusions; however, some remarkable observations can be made. First, some loose correlation can be suspected from most of the data points, as indicated by the full lines. According to these, the graphitic phase appears to be almost independent of and the other two carbon species seem to exhibit comple-

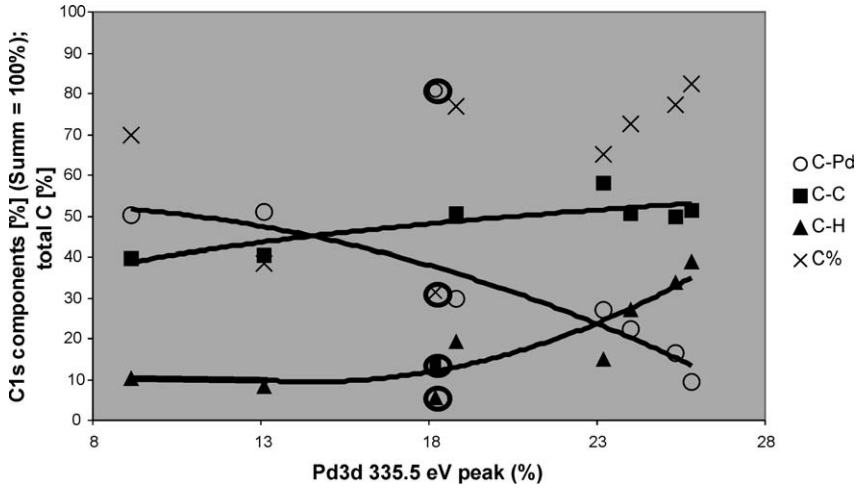

Fig. 8. Correlation of the total carbon content and the relative amounts of the individual carbon types as a function of the relative amount of adsorbed-induced Pd 3d component. Pd foil data are included. Most of the data points originate from Figs. 2 and 4.

mentary positive and negative correlations with the 335.5-eV palladium component. Surprisingly, the C–Pd species shows a negative correlation and the C–H component a positive correlation with the adsorbate-induced surface Pd peak. Second, the first data point after the cleaning procedure in high vacuum (indicated by circled symbols) absolutely does not fit into the trend lines, demonstrating that UHV and in situ (with gas phase) conditions might differ quite strongly from each other (pressure gap).

4. Discussion

In the previous section we presented XP spectra for varying gas-phase environments at different temperatures that demonstrated the dynamic behavior of the surface in the palladium system. These changes were detectable only in situ; no "postmortem" examination reveals the alterations. This was demonstrated unequivocally in Fig. 5, where the two successive scans on Pd 3d show different spectra; the surface oxide could be observed only in O_2 ambient and decomposed rapidly in high vacuum, leaving behind pure metallic palladium. Because of the background pressure of 10^{-7} mbar, however, the surface quickly becomes contaminated by carbonaceous species. An additional source of carbon accumulation is a beam-enhanced deposition of carbon containing molecules from the gas-phase background. The possibility of such quick surface contamination is therefore the price to pay for the use of non-UHV XPS chambers. In our opinion, however, this is the only way to perform XPS measurements in an environment that mimicks realistic catalytic conditions.

We identified three main types of surface carbon in our system: carbon in interaction with palladium, carbon connected to carbon, and "hydrogenated" carbon. The hydrogen content of the carbonaceous deposit depends on the hydrogen pressure and the temperature; higher $p(H_2)$ and lower temperature favor the formation of C–H species. At elevated temperatures the hydrogen content is low and the C–Pd component is increased. The spectrum measured in 4 mbar H_2 at 623 K indicates that the rate of C–H bond cleavage is much faster than its generation, and hydrogen readily desorbs (not surprisingly) at this T.

We have seen that at higher temperature (mainly C–C and C–Pd are present) the adsorbate-induced surface Pd component (BE 335.5 eV) is small (9–11%), although the total carbon content is still very high (up to 70%). This apparent contradiction can be explained by the assumption that part of the carbon is located not directly on the palladium surface but in 3D graphitic islands, and part of the carbon is atomically dispersed in the subsurface region. The higher C–Pd component on the foil indicates a more corrugated palladium surface with carbon in an in/subsurface position. The loose negative correlation between the surface-related adsorbate-induced Pd component (Pd 3d) and the C–Pd (C 1s) strengthens the localization of C–Pd not to the surface but to the subsurface region. The defect-rich polycrystalline surface ensures efficient carbon infiltration, which leads to expansion of the palladium lattice (see paragraph about HRTEM in Part II). Considering the presence of subsurface carbon, the C–Pd to C–H transformation can be explained by the direct hydrogenation of atomically dispersed carbon and by a more complex process, hydrogen entering the subsurface position, replacing carbon, which then will either be pushed deeper into the bulk or up to the surface, where its hydrogenation can take place.

The Pd(111) single crystal hydrogenated its carbon deposit much more weakly than the polycrystalline foil did, although the carbon content on the foil was approximately twice as high. Assuming that the rate of hydrogen dissociation is much faster on palladium (even in its highly covered state) than on the carbonaceous deposits, the polycrystalline sample promotes the (re)hydrogenation of the (sub)surface carbon much more strongly than does Pd(111). The palladium foil interacts with the carbon more "intimately,"

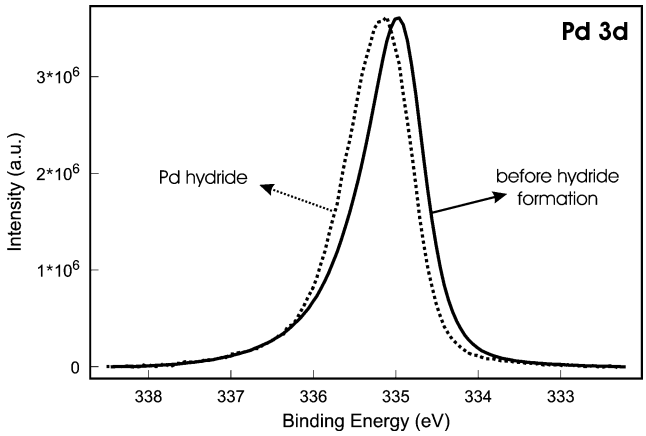

Fig. 9. Pd $3d_{(5/2)}$ of Pd foil before hydride formation and as a β hydride.

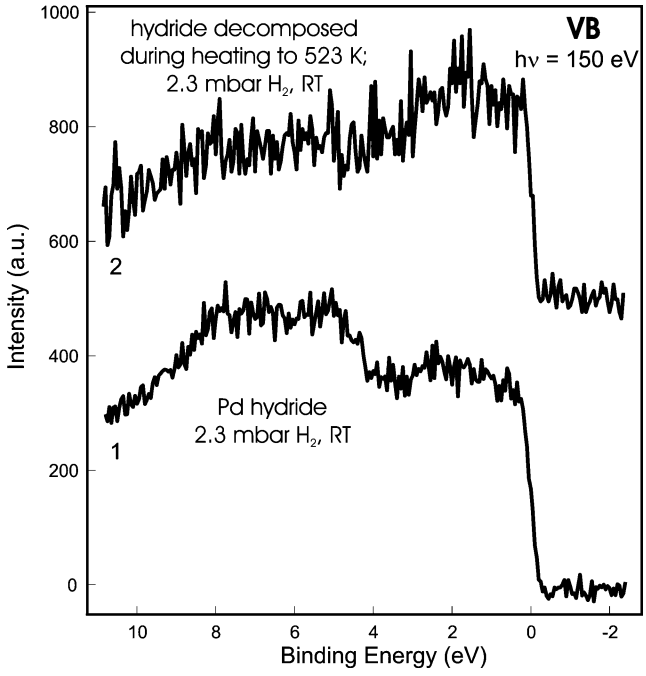

Fig. 10. Valence band of Pd foil in the β hydride state (1) and after hydride decomposition (2). RT and $\sim$ 2.3 mbar H_2.

which can be deduced from the higher abundance of C–Pd species on the foil and from the above-mentioned higher rehydrogenation ability.

Hydrogen interacts with palladium, readily giving rise to adsorbed and absorbed phases. The equilibrium diagram of the palladium–hydrogen system with the two homogeneous hydride phases (α and β) and the heterogeneous two phases below the critical temperature is well known [29,71,72]. However, in "surface science" conditions, as demonstrated by ongoing debates about different hydrogen species, the observed patterns (TDS, LEED, HREEL, etc.) strongly depend on the sample and adsorption temperature, on the introduced amount of hydrogen, on the surface cleanness, and partly on the exposed surface. Under our experimental conditions, with $p(H_2)$ in the mbar range, palladium is expected to be in the α phase; the equilibrium pressure for the transition toward the β phase at RT is about 7–10 mbar. There are no XPS data in the literature for the two hydride phases under realistic conditions. The available measurements [73–75] were made after the β phase ($PdH_{\sim 0.6}$) was generated at RT and the temperature was brought down to $\sim$ 100 K, at which point the equilibrium pressure is in UHV. The results indicated that the d-band is modified and shifted relative to E_F, that the density of states at E_F decreases, a new hydrogen-induced band is formed about 7–8 eV below E_F, and the Pd 3d core level shifts by about +0.2 eV to higher BE and becomes more symmetrical. According to these papers, all of these findings should correspond to the β phase, whereas no information is obtained for the α phase. Our results resemble none of the literature findings. (For a discussion of the valence band spectra see Part II.) Therefore, if the literature data are transferable to catalytically realistic temperatures, our measurements were made in the α phase regime and the α phase does not exhibit the above spectroscopic pattern. In addition, we have carried out experiments to generate and measure the β hydride phase as well. It is well known [29,71] that the α/β transformation exhibits a characteristic hysteresis. The decomposition of the β phase takes place at lower equilibrium hydrogen pressure than its generation. Therefore once this phase is produced, there might be a chance to measure it at pressures that were not high enough for generation. The preparation we used is explained in the Experimental section. Figs. 9 and 10 show, respectively, the Pd 3d and valence band region of the palladium foil, after the atmospheric hydrogen treatment but in 2.3 mbar hydrogen. The 3d core level displays after the β phase is generated a 0.18-eV binding energy shift, and the asymmetry of the peak decreased, as was shown at low T and predicted by the theory [31,73,74]. Although the quality of the VB spectra is very poor, the similarity to the low-temperature data concerning the hydrogen-induced band is obvious. This band was absent after the sample was heated to 523 K. Therefore these features are also characteristic of the β hydride at room temperature.

5. Conclusion

High-pressure XPS is an excellent tool for the study of the electronic structure of catalysts under gas ambient in the mbar pressure range. We demonstrated that the surface is dynamic and always reflects its ambient (gas phase, pressure, temperature). Surface oxide was observed on Pd(111) at 573 K, which decomposed as the oxygen supply was switched off. Because of the high surface sensitivity of XPS, impurity accumulation under non-UHV conditions (non-UHV chamber, non-infinite gas purity) is increased. Carbon accumulated on palladium from the gas base-pressure of the chamber. However, the carbonaceous layer on the surface

was strongly influenced by the presence of hydrogen and by the temperature. Few (1–4) mbar of hydrogen was not enough to form palladium β hydride. On the other hand, by making use of the hysteresis of the α/β transformation, it is possible to stabilize the β phase in this pressure range. Its spectroscopic characteristics seem to be similar to literature data recorded at ~ 100 K.

Acknowledgments

Financial support from the ATHENA Project is gratefully acknowledged. One of us also thanks the Humboldt Foundation for the Roman-Herzog-Stipendium. In addition, we thank the BESSY staff for their continual support during the XPS measurements.

References

[1] R.A. Dalla Betta, K. Tsurumi, Shoji, US Patent 5258349 (1993).
[2] S. Morikawa, S. Samejima, M. Yoshitake, N. Tatematsu, Jpn. Patent 3-099026 (1991).
[3] J. Moore, J. O'Kell, EU Patent 508660 (1992).
[4] A. Chauvel, G. Lefebvre, Petrochemical Processes 2 (1989) 36.
[5] Hoechst, EP. 330853 (1989), EP. 403950 (1990), EP. 431478 (1991), EP. 519435 (1992).
[6] R.B. Anderson, K.C. Stein, J.J. Feenan, L.E.J. Hofer, Ind. Eng. Chem. 53 (1961) 809.
[7] W.K. Lam, L. Lloyd, Oil Gas 27 (1972) 66.
[8] G.C. Bond, P.B. Wells, Adv. Catal. 15 (1964) 91.
[9] T. Mallat, A. Baiker, Catal. Today 19 (1994) 247.
[10] M.L. Derrien, Stud. Surf. Sci. Catal. 27 (1986) 613.
[11] D. Stacchiola, S. Azad, L. Burkholder, W.T. Tysoe, J. Phys. Chem. B 105 (2001) 11233.
[12] B. Heinrichs, J.-P. Schoebrechts, J.-P. Pirard, J. Catal. 200 (2001) 309.
[13] G.B. Hoflund, H.A.E. Hagelin, J.F. Weaver, G.N. Salaita, Appl. Surf. Sci. 205 (2003) 102.
[14] C.F. Cullis, B.M. Willatt, J. Catal. 83 (1982) 267.
[15] J.H. Kang, E.W. Shin, W.J. Kim, J.D. Park, S.H. Moon, J. Catal. 208 (2002) 310.
[16] W.-J. Shen, Y. Ichihashi, H. Ando, Y. Matsumara, M. Okumura, M. Haruta, Appl. Catal. A 217 (2001) 231.
[17] A. Trovarelli, Catal. Rev.-Sci. Eng. 38 (1996) 439.
[18] G. Tourillon, A. Cassuto, Y. Jugnet, J. Massardier, J.C. Bertolini, J. Chem. Soc., Faraday Trans. 92 (1996) 4835.
[19] A. Sandell, A. Beutler, A. Jaworowski, M. Wiklund, K. Heister, R. Nyholm, J.M. Andersen, Surf. Sci. 415 (1998) 411.
[20] U. Muschiol, P.K. Schmidt, K. Christmann, Surf. Sci. 395 (1998) 182.
[21] Sh. Shaikhutdinov, M. Heemeier, M. Bäumer, T. Lear, D. Lennon, R. Oldman, S.D. Jackson, H.-J. Freund, J. Catal. 200 (2001) 330.
[22] D.R. Lloyd, C.M. Quinn, N.V. Richardson, Surf. Sci. 63 (1977) 174.
[23] S. Surnev, M. Sock, M.G. Ramsey, F.P. Netzer, M. Wiklund, M. Borg, J.N. Andersen, Surf. Sci. 470 (2000) 171.
[24] T. Mitsui, M.K. Rose, E. Fomin, D.F. Ogletree, M. Salmeron, Nature 422 (2003) 705.
[25] G. Alefeld, J. Völkl (Eds.), Hydrogen in Metals I and II (Topics in Applied Physics), Springer, Berlin, 1978, pp. 28–29.
[26] L. Schlapbach, A. Züttel, P. Gröning, O. Gröning, P. Aebi, Appl. Phys. A 72 (2001) 245.
[27] J.-F. Paul, P. Sautet, Phys. Rev. B 53 (1996) 8015.
[28] Z. Király, Á. Mastalir, F. Berger, I. Dékány, Langmuir 13 (1997) 465.
[29] H. Frieske, E. Wicke, Ber. Bunsenges. 77 (1973) 48.
[30] G.E. Gdowski, T.E. Felter, R.H. Stulen, Surf. Sci. 181 (1987) L147.
[31] W. Eberhardt, S.G. Louie, E.W. Plummer, Phys. Rev. B 28 (1983) 465.
[32] W. Auer, H.J. Grabke, Ber. Bunsenges. 78 (1974) 58.
[33] S.G. Louie, Phys. Rev. Lett. 40 (1978) 1515.
[34] R.J. Rennard, R.J. Kokes, J. Phys. Chem. 70 (1966) 2543.
[35] H. Molero, B.F. Bartlett, W.T. Tysoe, J. Catal. 181 (1999) 49.
[36] Z. Paál, in: Z. Paál, P.G. Menon (Eds.), Hydrogen Effect in Catalysis, Dekker, New York, 1988.
[37] D. Teschner, D. Duprez, Z. Paál, J. Mol. Catal. 179 (2002) 201.
[38] M. Kaltchev, D. Stacchiola, H. Molero, G. Wu, A. Blumenfeld, W.T. Tysoe, Catal. Lett. 60 (1999) 11.
[39] F. Zaera, Mol. Phys. 100 (2002) 3065.
[40] J.A. Gates, L.L. Kesmodel, Surf. Sci. 124 (1983) 68.
[41] W.T. Tysoe, G.L. Nyberg, R.M. Lambert, J. Phys. Chem. 90 (1986) 3188.
[42] B. Hugenschmidt, P. Dolle, J. Jupille, A. Cassuto, J. Vac. Sci. Technol. A 7 (1989) 3312.
[43] Y.R. Shen, Nature 337 (1989) 519.
[44] B.J. McIntyre, M. Salmeron, G.A. Somorjai, Rev. Sci. Instrum. 64 (1993) 687.
[45] C. Sachs, M. Hillebrand, S. Völkening, J. Wintterlin, G. Ertl, Science 293 (2001) 1635.
[46] T.W. Hansen, J.B. Wagner, P.L. Hansen, S. Dahl, H. Topsoe, C.J.H. Jacobson, Science 294 (2001) 1508.
[47] J.F. Haw, J.B. Nicholas, T. Xu, L.W. Beck, D.B. Ferguson, Acc. Chem. Res. 29 (1996) 259.
[48] H. Knözinger, G. Mestl, Top. Catal. 8 (1999) 45.
[49] A. Knop-Gericke, M. Hävecker, T. Schedel-Niedrig, R. Schlögl, Top. Catal. 15 (2001) 27.
[50] R.W. Joyner, M.W. Roberts, Chem. Phys. Lett. 60 (1979) 459.
[51] G.A. Somorjai, G. Rupprechter, J. Phys Chem. B 103 (1999) 1623.
[52] F. Garin, G. Maire, S. Zyade, M. Zauwen, A. Frennet, P. Zielinski, J. Mol. Catal. 58 (1990) 185.
[53] H. Bluhm, M. Hävecker, A. Knop-Gericke, E. Kleimenov, R. Schlögl, D. Teschner, V.I. Bukhtiyarov, D.F. Ogletree, M. Salmeron, J. Phys. Chem. B, in press.
[54] V.V. Kaichev, I.P. Prosvirin, V.L. Bukhtiyarov, H. Unterhalt, G. Rupprechter, H.-J. Freund, J. Phys. Chem. B 107 (2003) 3522.
[55] V.I. Bukhtiyarov, I.P. Prosvirin, E.P. Tikhomirov, V.V. Kaichev, A.M. Sorokin, V.V. Evstigneev, React. Kinet. Catal. Lett. 79 (2003) 181.
[56] V.I. Bukhtiyarov, Kinet. Catal. 44 (2003) 420.
[57] H.-J. Ruppender, M. Grunze, C.W. Kong, M. Wilmers, Surf. Interface Anal. 15 (1990) 245.
[58] D.F. Ogletree, H. Bluhm, G. Lebedev, C. Fadley, Z. Hussain, M. Salmeron, Rev. Sci. Instrum. 73 (2002) 3872.
[59] S. Doniach, M. Sunjic, J. Phys. C 3 (1970) 285.
[60] J.J. Yeh, I. Lindau, At. Data Nucl. Data Tables 32 (1985) 1.
[61] S. Tanuma, C.J. Powell, D.R. Penn, Surf. Interface Anal. 17 (1991) 911.
[62] K.S. Kim, A.F. Gossmann, N. Winograd, Anal. Chem. 46 (1974) 197.
[63] M. Todorova, E. Lundgren, V. Blum, A. Mikkelsen, S. Gray, J. Gustafson, M. Borg, J. Rogal, K. Reuter, J.N. Andersen, M. Scheffler, Surf. Sci. 541 (2003) 101.
[64] E. Lundgren, G. Kresse, C. Klein, M. Borg, J.N. Andersen, M. De Santis, Y. Gauthier, C. Konvicka, M. Schmid, P. Varga, Phys. Rev. Lett. 88 (2002) 2461031.
[65] G.A. Somorjai, F. Zaera, J. Phys. Chem. 8 (1982) 3070.
[66] N.M. Rodriguez, P. Anderson, Z. Paál, U. Wild, A. Wootsch, R. Schlögl, J. Catal. 197 (2001) 365.
[67] Z. Paál, U. Wild, R. Schlögl, Phys. Chem. Chem. Phys. 3 (2001) 4644.
[68] Z. Paál, R. Schlögl, G. Ertl, J. Chem. Soc. Faraday Trans. 88 (1992) 1179.

[69] I.V. Yudanow, K.M. Neyman, N. Rösch, Phys. Chem. Chem. Phys. 6 (2004) 116.
[70] J.N. Andersen, D. Henning, E. Lundgren, M. Methfessel, R. Nyholm, M. Scheffler, Phys. Rev. B 50 (1994) 17525.
[71] F.A. Lewis, The Palladium–Hydrogen System, Academic Press, New York, 1967.
[72] R.J. Wolf, M.W. Lee, R.C. Davis, P.J. Fay, J.R. Ray, Phys. Rev. B 48 (1993) 12415.
[73] P.A. Bennett, J.C. Fuggle, Phys. Rev. B 26 (1982) 6030.
[74] L. Schlapbach, J.P. Burger, J. Physique 43 (1982) L273.
[75] F. Antonangeli, A. Balzarotti, A. Bianconi, P. Perfetti, Solid State Commun. 21 (1977) 201.